

Fast AC Power Flow Optimization using Difference of Convex Functions Programming

Sandro Merkli^{*†}, Alexander Domahidi^{‡†}, Juan Jerez^{*‡}
Manfred Morari^{*}, Roy S. Smith^{*}

July 27, 2016

An effective means for analyzing the impact of novel operating schemes on power systems is time domain simulation, for example for investigating optimization-based curtailment of renewables to alleviate voltage violations. Traditionally, interior-point methods are used for solving the non-convex AC optimal power flow (OPF) problems arising in this type of simulation. This paper presents an alternative algorithm that better suits the simulation framework, because it can more effectively be warm-started, has linear computational and memory complexity in the problem size per iteration and globally converges to Karush-Kuhn-Tucker (KKT) points with a linear rate if they exist. The algorithm exploits a difference-of-convex-functions reformulation of the OPF problem, which can be performed effectively. Numerical results are presented comparing the method to state-of-the-art OPF solver implementations in MATPOWER, leading to significant speedups compared to the latter.

1. Introduction

The amount of renewable energy sources (RES) in distribution systems is steadily increasing [25]. Due to their volatility and limited predictability, they are posing new challenges to power system operation and planning. A prominently observed consequence of the increase in renewable power in-feeds are local voltage limit violations [4]. Traditionally, the remedy for these violations required expensive line capacity extensions. Recent studies have shown that such extensions could be reduced by a shift in operational paradigms from rule-based to optimization-based approaches, see for example [31,32,34].

*Automatic Control Lab, ETH Zurich, Physikstrasse 3, 8092 Zurich
{merkli,smith,juanj}@control.ee.ethz.ch

†Inspire-IfA, Inspire AG, Technoparkstrasse 1, 8005 Zurich. {merkli,domahidi}@inspire.ethz.ch

‡embotech GmbH, Physikstrasse 3, ETL K10.1, 8092 Zurich, {jerez,domahidi}@embotech.com

Since it is non-trivial to predict the impact of such shifts in operational paradigms on power systems, time-domain simulations provide valuable insight [31]. System-wide simulations over extended periods of time can demonstrate seasonal impacts and yield statistical data. This data provides a more in-depth view than worst-case snapshot studies, which are the current industrial practice. While the latter only provides information on violation severity, the former also gives a sense of how often they occur. However, if the impact of optimization-based approaches is to be simulated over such long periods of time and for different scenarios, a large number of optimization problems need to be solved. In the case of dispatch optimization, sampling times for the control are on the order of 15 minutes. This means that proposed optimization problems can typically be solved fast enough for on-line operation using state-of-the-art software such as MATPOWER [35]. However, in simulations, solving the optimization problems is the most computationally expensive task. Therefore, efficient numerical methods are essential for performing simulations in a practical time frame.

In many cases, the problems proposed in optimization-based operation schemes are related to a class of problems collectively referred to as optimal power flow (OPF) problems. An extensive amount of literature exists on solving such problems and a recent survey is given in [11,12]. However, due to the non-convexity and large scale of the problem, it remains an active research topic. In fact, the non-convexity makes the problem computationally intractable to solve to global optimality in general. However, critical points can in most cases be found efficiently if they exist, for example using sequential quadratic programming (SQP) [27] and an initial guess that is close to the critical point, or with the difference-of-convex-functions method used in this paper [20]. The most popular approaches to solving AC OPF problems are interior point methods [30] and sequential convex approximation methods [1, 7]. While the former are numerically robust and well-studied, the latter tend to be faster according to [11]. There are two main sequential convex approximation approaches: Sequential linear programming (SLP) and SQP. These schemes approximate the original problem iteratively with convex linear and quadratic programs, respectively. Most implementations of these approaches use conventional power flow computations between their iterations to restore feasibility of the Kirchhoff equations. In general, SLP/SQP methods require extensions to become globally convergent, which reduces their performance [11]. A recently developed alternative approach is to solve a convex semidefinite programming (SDP) relaxation of the problem [19,22]. The optimal value of this relaxation is either the globally optimal value of the non-convex problem or in the worst case only a lower bound on the latter.

The reformulation presented in this paper allows for the solution of AC optimal power flow problems using difference of convex functions programming. This higher order approximation is tighter than the one made in SLP/SQP methods. In comparison with SLP, the method has no issues of unboundedness of the relaxations and is globally convergent without extensions. The presented method operates entirely in the voltage space, satisfying the Kirchhoff equations by design and thereby eliminating the need for conventional power flow computations. In comparison with the SDP relaxation, it converges to critical points at a lower computational cost than the former, especially when warm-started. Also, the SDP relaxation provides only a lower bound on the

objective in the worst case, which does not provide a feasible point. In contrast, the proposed method always converges to a critical point if one exists. While certifying local optimality of these points is not straightforward, experiments show that they represent acceptable solutions. This statement will be quantified in the numerical results section.

In this work, we present the application of our method to a specific example of an optimization-based operation scheme designed to reduce RES curtailments. In this example, the distribution system operator (DSO) is tasked with keeping the system stable and within the allowed operating conditions. Normally, the DSO is not operated for financial gain and its actions are bound to regulations, for example the EEG in Germany [6] or the European equivalent ENTSO [9]. The range of actions the DSO can take includes adjusting setpoints of generators and curtailing renewable energy sources. Approaches for finding such points currently used in practice are usually rule-based. Such rules involve a significant amount of tuning and rarely come with mathematical guarantees. Additionally, costs for adjustments can only indirectly be taken into account.

While the rest of the paper is developed with this specific example in mind, the theory applies to a wide range of problems involving similar constraints, including standard economic dispatch. In particular, any AC power flow optimizations can make use of the decomposition technique presented here.

1.1. Summary of contribution

In this paper, we present a novel method for solving a class of optimal power flow problems that is particularly suited for time-domain system simulations.

- (i) *Formulation*: We propose an OPF-like optimization problem to reduce curtailment in distribution grid operation. While the constraints are similar to economic dispatch, the cost function is formulated specifically to represent the cost faced by the system operator.
- (ii) *Reformulation into a difference-of-convex functions problem*: We give an efficient method for transforming the given OPF problem into a difference of convex functions problem. Its computational complexity is linear in the problem size. This reformulation preserves the sparsity of the problem while at the same time leading to the sequential convex relaxations being as close to the original non-convex problem as possible within the DC programming framework.
- (iii) *Efficient solution of convex subproblems*: The difference of convex functions approach solves the non-convex problem using a series of convex approximations, in this case second-order cone programs (SOCPs) that can be reformulated as convex quadratically constrained linear problems (QCLPs). We present an approach using accelerated dual projected gradient methods to solving these QCLPs that exploits their structure. This leads to the complexity of all iteration computations as well as the required amount of memory growing linearly with the problem size.

1.2. Outline

The rest of this paper is structured as follows: Section 2 introduces some preliminaries. In Section 3, we present a reformulation of the optimization problem such that the difference-of-convex-functions method is applicable. Section 4 outlines an efficient method to solve the convex inner problems arising in the proposed algorithm. In Section 5, numerical results are presented and discussed. Final conclusions are presented in Section 6.

2. Preliminaries

This section outlines both the model of the power system as well as the optimization-based control strategy we propose. Basic notation is introduced, assumptions are clarified and current operational practice is described.

2.1. Notation

The power grid is modeled as an undirected graph with M vertices and L edges. Vertices model buses, while edges model power lines. Each line (say, from bus j to bus l) has admittance $y_{jl} \in \mathbb{C}$. Each bus j has an associated voltage $v_j \in \mathbb{C}$ and power in-feed $s_j \in \mathbb{C}$, where $\text{Re}(s_j)$ denotes active and $\text{Im}(s_j)$ denotes reactive power. Let $v, s \in \mathbb{C}^M$ be the stacked versions of the bus voltages and powers, respectively. The admittance matrix of the grid is given as

$$Y_{jl} := \begin{cases} y_{jl} & \text{if } j \neq l, \\ y_j^{\text{sh}} - \sum_{k=1, k \neq j}^M y_{jk} & \text{if } j = l. \end{cases} \quad (1)$$

where $y_j^{\text{sh}} \in \mathbb{C}$ are shunt admittances. The Kirchoff equations for the system can hence be written in matrix form:

$$\text{diag}(v) \bar{Y} \bar{v} = s, \quad (2)$$

where $\bar{\cdot}$ describes the (element-wise) complex conjugate. Let e_k denote the k -th unit vector with appropriate dimension. Let $(\cdot)^r := \text{Re}(\cdot)$, $(\cdot)^q := \text{Im}(\cdot)$ and let r_k, q_k be the k -th rows of $\text{Re}(Y)$ and $\text{Im}(Y)$, respectively. For vectors $a \in \mathbb{C}^n$, define

$$J(a) := \left\{ k \in \{1, \dots, n\} \mid a_k \neq 0 \right\}, \quad (3)$$

and for matrices $A \in \mathbb{C}^{n \times n}$, let

$$J(A) := \left\{ k \in \{1, \dots, n\} \mid \exists j \in \{1, \dots, n\} : A_{kj} \neq 0 \text{ or } A_{jk} \neq 0 \right\}. \quad (4)$$

This means $J(\cdot)$ returns the indexes of rows and columns with at least one nonzero entry. We then use the notation A_B to denote a version of A with only the rows and columns with indexes from a given set B .

2.2. Operational constraints

The constraints represent limits introduced by the system operator are either due to regulations or to avoid damage to the system. Firstly, the voltage magnitude has to be within a fixed interval for each bus j :

$$v_{\min,j} \leq |v_j| \leq v_{\max,j}. \quad (5)$$

These limits are important for distribution grids, since the assumption of low-resistance lines commonly made in transmission grids does not hold. This means there can be significant discrepancies in the voltages between two endpoints of a line. Additionally, one of the main problems faced by DSOs are voltage constraint violations due to local renewable power in-feeds. Finally, the current through each line (j, k) is limited for thermal reasons:

$$|y_{jl}| |v_j - v_l| \leq i_{\max,jl}, \quad (6)$$

The limits in (5) and (6) together will hereafter be referred to as the operational constraints for the power grid. The DSO action space is modeled as an interval of active and reactive power for each bus j :

$$\begin{aligned} p_{\min,j} \leq \operatorname{Re}(s_j) \leq p_{\max,j}, \\ q_{\min,j} \leq \operatorname{Im}(s_j) \leq q_{\max,j}. \end{aligned} \quad (7)$$

For buses at which the DSO cannot intervene, the upper and lower limits in (7) are equal. Let (s^0, v^0) be an operating point of the power grid that represents the state of the distribution grid without any DSO intervention. If this point satisfies all operational constraints (5) and (6), no DSO intervention is required. Otherwise, some limits are violated and the task of the DSO is then to find a point (s, v) that satisfies all operational constraints, but also lies within its action space (7).

2.3. DSO optimization problem

The penalization for introduced deviations to power setpoints is modeled linearly here, while voltage deviations are interpreted as an effect of changing powers without a direct cost. This is the case for example in Germany [6]. Even though the DSO is not run for profit, its operational cost has to be covered by the power consumers. It is therefore advisable to perform a social welfare optimization for least cost:

$$\underset{s \in \mathbb{C}^M, v \in \mathbb{C}^M}{\text{minimize}} \quad \|\operatorname{Re}(s - s_0)\|_1 + \|\operatorname{Im}(s - s_0)\|_1 \quad (8a)$$

$$\text{subject to} \quad \operatorname{diag}(v) \bar{Y} v = s, \quad (8b)$$

$$v_{\min,k} \leq |v_k| \leq v_{\max,k}, \quad (8c)$$

$$p_{\min} \leq \operatorname{Re}(s) \leq p_{\max}, \quad (8d)$$

$$q_{\min} \leq \operatorname{Im}(s) \leq q_{\max}, \quad (8e)$$

$$|y_{jl}| |v_j - v_l| \leq i_{\max,(j,l)}, \quad (8f)$$

$$k \in \mathcal{M}, \quad (j, l) \in \mathcal{E}, \quad (8g)$$

where the 1-norm cost function is proportional to the monetary cost for the power deviations the DSO introduces. For renewable in-feed curtailment, this situation is commonplace in some European countries, where the operator is typically required by law to pay the nominal price for available power, regardless of whether it is used or curtailed. Since this is the most relevant case here, the assumption is made that all costs are of this structure. However, the general framework presented in this work can be extended to use any convex cost function. Problem (8) will hereafter be referred to as the OPF problem. It is non-convex due to the quadratic Kirchhoff equalities (8b) as well as the lower voltage magnitude bounds (8c).

2.4. Difference-of-convex-functions (DC) programming

The method used in this work for solving problem (8) is called difference-of-convex-functions (DC¹) programming. This section outlines the algorithm and presents some existing related theoretical results. DC programming is a class of algorithms for solving problems of the form

$$\begin{aligned} & \underset{x}{\text{minimize}} && g_0(x) - h_0(x) \\ & \text{subject to} && g_i(x) - h_i(x) \leq 0, \end{aligned} \tag{9}$$

where $i \in \{1, \dots, m\}$ and the g_i, h_i are convex, subdifferentiable functions. This method was historically used for optimization problems involving piecewise affine functions. However, a wide range of problems can be formulated as (9), including all convex optimization problems, optimization problems with binary variables, quadratic equality constraints and higher-order polynomial constraints. A recent survey of the method and related theory is given in [2], and [20] presents the basic algorithm, which is also given in Algorithm 1 for completeness. The main idea of the algorithm is to solve a sequence of convex problems obtained by linearizing the *concave* parts of the constraints and objective:

$$\begin{aligned} & \underset{x}{\text{minimize}} && g_0(x) - [h_0(\tilde{x}) + \nabla h_0(\tilde{x})(x - \tilde{x})] \\ & \text{subject to} && g_i(x) - [h_i(\tilde{x}) + \nabla h_i(\tilde{x})(x - \tilde{x})] \leq 0. \end{aligned} \tag{10}$$

The optimizer x^* of (10) is then used as the next point of convexification \tilde{x} , and the process is repeated until convergence is reached. The feasible set of (10) is a convex inner approximation of that of (9). This means that (10) is not necessarily feasible, even if the original non-convex problem is. This is circumvented in the algorithm using a penalty reformulation:

$$\begin{aligned} & \underset{x,t}{\text{minimize}} && g_0(x) - [h_0(\tilde{x}) + \nabla h_0(\tilde{x})(x - \tilde{x})] + \beta^k t \\ & \text{subject to} && g_i(x) - [h_i(\tilde{x}) + \nabla h_i(\tilde{x})(x - \tilde{x})] \leq t, \\ & && t \geq 0, \end{aligned} \tag{11}$$

¹Not to be confused with the abbreviation ‘‘DC’’ for direct current, and the related approximations of the AC-OPF problem.

```

1: Let  $x^0$  initial guess,  $\beta^0, \delta_1, \delta_2 > 0$  parameters,  $\epsilon_x, \epsilon_t > 0$  tolerances
2: while Not converged do
3:    $x^{k+1}, \lambda^{k+1}, t^* \leftarrow$  Solution of (11)
4:   if  $\|x^{k+1} - x^k\| \leq \epsilon_x$  and  $t \leq \epsilon_t$  then
5:     Terminate, converged to local optimality.
6:   end if
7:    $r^k \leftarrow \min \left\{ (\|x^{k+1} - x^k\|_2)^{-1}, \|\lambda^{k+1}\|_1 + \delta_1 \right\}$ 
8:    $\beta^{k+1} \leftarrow \begin{cases} \beta^k & \text{if } \beta^k \geq r^k \\ \beta^k + \delta_2 & \text{if } \beta^k < r^k \end{cases}$ 
9: end while

```

Fig. 1: Difference of convex functions algorithm from [20], modified to use practical stopping criteria. The λ^{k+1} computed in Step 3 is the vector of dual multipliers of the constraints of the inner problem.

where $\beta^k \in \mathbb{R}_+$ is a penalty weight parameter that is updated after each convexification using the rule in Algorithm 1.

Note the similarity of this scheme to other sequential convex programming methods, most notably SQP and SLP. The key difference to those methods is that the convex parts g_i are retained in their original form, which yields tighter approximations in the sequence of convex problems solved. This means in particular that if the original problem had a bounded feasible set, all issues of possible unboundedness that arise in SLP [5] are avoided and there is no need for trust region approaches and their associated performance penalty.

It is shown in [20] that the algorithm presented here globally converges to a KKT point of (9) with a linear rate, provided one exists and standard constraint qualifications are satisfied. It is also shown that the sequence of optimal values of the approximations (11) is monotonically decreasing. This holds for all initial choices of the algorithm parameters, which means no a priori bound on the size of the penalty parameter β_k is required. All results also hold if, in addition to the constraints in (9), a constraint

$$x \in \mathcal{C}, \tag{12}$$

for some convex, closed set \mathcal{C} is added. The algorithms are then simply modified to include the constraint (12) in each of the convex approximations. It is worth noting that the choice of g_i and h_i is not unique for a given problem. The authors in [20] make no theoretical statements on the impact of the choice of the g_i and h_i on the convergence speed. However, numerical experiments show that the choice does have a strong impact on the number of iterations required. We will discuss an effective technique for choosing the functions g_i, h_i for the problem at hand in Section 3.2.

3. Reformulation of OPF as Difference-of-Convex-functions problem

In this section, the DSO OPF problem (8) is reformulated as a QCLP, and an efficient way of computing the splits of the non-convex functions into differences of convex functions is presented. These splits result in a special structure of the convex sub-problems. We then show in Section 4 how to solve these sub-problems efficiently.

3.1. Reformulation as QCLP

As already shown in [21], OPF problems with linear cost functions can be recast as non-convex quadratically constrained linear programs. A similar technique will be applied here. First, let $s_0 \in \mathbb{C}^M, v_0 \in \mathbb{C}^M$ be the power and voltage vectors the system is operating at without any DSO intervention. We now introduce the difference in voltages introduced by the DSO as follows:

$$v := v_0 + \Delta v \in \mathbb{C}^M, \quad (13)$$

where $\Delta v \in \mathbb{C}^M$ is the change from the starting point and v is the resulting voltage vector. The resulting change of powers $\Delta s \in \mathbb{C}^M$ can be computed using the Kirchhoff equations (8b):

$$\Delta s = \text{diag}(v_0)\bar{Y}\bar{\Delta}v + \text{diag}(\Delta v)\bar{Y}\bar{v} + \text{diag}(\Delta v)\bar{Y}\bar{\Delta}v.$$

Define now $Y^{(k)}$ as a version of Y with all but the k -th row set to 0. After some reformulation, we can write

$$\left(\text{Re}(\Delta s) \right)_k = z^T H_{r,k} z + h_{r,k}^T z, \quad (14a)$$

$$\left(\text{Im}(\Delta s) \right)_k = z^T H_{q,k} z + h_{q,k}^T z, \quad (14b)$$

with $z := [\text{Re}(\Delta v)^T \quad \text{Im}(\Delta v)^T]^T \in \mathbb{R}^{2M}$, and

$$\begin{aligned} H_{r,k} &:= \begin{bmatrix} \text{Re}(Y^{(k)}) & -\text{Im}(Y^{(k)}) \\ \text{Im}(Y^{(k)}) & \text{Re}(Y^{(k)}) \end{bmatrix}, \\ H_{q,k} &:= \begin{bmatrix} -\text{Im}(Y^{(k)}) & -\text{Re}(Y^{(k)}) \\ \text{Re}(Y^{(k)}) & -\text{Im}(Y^{(k)}) \end{bmatrix}. \end{aligned} \quad (15)$$

The linear parts in (14) are given by

$$\begin{aligned}
h_{r,k} &:= \\
&\begin{bmatrix} \left((v_0^r)_k r_k + (v_0^q)_k q_k \right)^T + e_k \left(r_k (v_0^r)_k + q_k (v_0^q)_k \right) \\ \left((v_0^q)_k r_k - (v_0^r)_k q_k \right)^T + e_k \left(q_k (v_0^r)_k + r_k (v_0^q)_k \right) \end{bmatrix}, \\
h_{q,k} &:= \\
&\begin{bmatrix} \left((v_0^q)_k r_k - (v_0^r)_k q_k \right)^T - e_k \left(q_k (v_0^r)_k + r_k (v_0^q)_k \right) \\ \left(- (v_0^q)_k q_k - (v_0^r)_k r_k \right)^T + e_k \left(r_k (v_0^r)_k - r_k (v_0^q)_k \right) \end{bmatrix}.
\end{aligned} \tag{16}$$

Equations (14) can now be used to express the constraints on powers given in (8d)–(8e) as constraints on Δv . Using (13), the constraints (8c) and (8f) can also be expressed in Δv . Finally, problem (8) can be rewritten entirely in the variable z :

$$\begin{aligned}
&\underset{z \in \mathbb{R}^{2M}}{\text{minimize}} \quad \sum_{k=1}^M |z^T H_{r,k} z + h_{r,k}^T z| + |z^T H_{q,k} z + h_{q,k}^T z| \tag{17a}
\end{aligned}$$

$$\begin{aligned}
&\text{subject to} \quad z^T Q_i z + q_i^T z + \gamma_i \leq 0, \tag{17b} \\
&\quad i \in \{1, \dots, K\},
\end{aligned}$$

where $K := 6M + L$. The constraints (17b) are reformulations of the original constraints (8c)–(8f). The structures of the Q_i are of particular importance in later sections, which is why they are given here.

- (i) The matrix Q of power constraints (8d) and (8e) are either the matrices $H_{r,k}$ or $H_{q,k}$ or negative versions thereof.
- (ii) For the voltage bounds (8c), Q has 1 (for upper bounds) or -1 (for lower bounds) on the j -th and $(M + j)$ -th entries on the diagonal, and 0 everywhere else.
- (iii) The matrix Q of line constraints (8f) have 1 in positions

$$(j, j), (l, l), (M + j, M + j), (M + l, M + l),$$

of the diagonal and -1 in positions

$$(j, l), (l, j), (M + j, M + l), (M + j, M + l).$$

Note that the matrices from (15) are not symmetric, but they can be trivially made symmetric without changing the value of the constraints in (17b). We hence define the symmetric versions

$$\hat{H}_{r,k} := \frac{H_{r,k} + H_{r,k}^T}{2}, \quad \hat{H}_{q,k} := \frac{H_{q,k} + H_{q,k}^T}{2}. \tag{18}$$

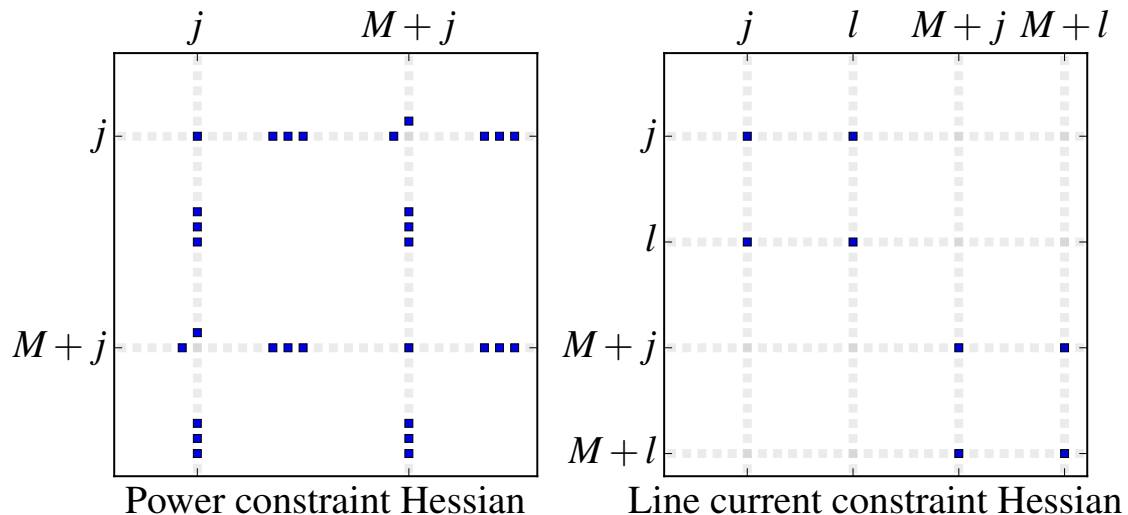


Fig. 2: Sparsity pattern of example power constraint and line constraint Hessian matrices Q . In this case, vertex j has 4 neighbors. Note that the power constraint matrix is shown in symmetric form as defined in (18).

A visualization of the described sparsity patterns is given in Figure 2. Since the cost function (17a) is inconvenient due to its non-smoothness, a standard 1-norm reformulation with additional slack variables $u \in \mathbb{R}^{2M}$ is performed. Defining $x := [z^T \ u^T]^T$, problem (17) can be written as a standard QCLP:

$$\underset{x}{\text{minimize}} \quad c^T x \tag{19a}$$

$$\text{subject to} \quad x^T P_i x + p_i^T x + \omega_i \leq 0, \tag{19b}$$

$$i \in \{1, \dots, 10M + L\},$$

$$x_j \geq 0, \tag{19c}$$

$$j \in \{2M + 1, \dots, 4M\},$$

for appropriate c, P_i, p_i, ω_i . The structure of the matrices P_i is given by

$$P_i = \begin{bmatrix} * & 0^{2M \times 2M} \\ 0^{2M \times 2M} & 0^{2M \times 2M} \end{bmatrix} \in \mathbb{R}^{4M \times 4M}, \tag{20}$$

where the upper blocks denoted by $*$ have the same sparsity patterns as the matrices from Problem (17). The vectors $p_i \in \mathbb{R}^{4M}$ are versions of the linear parts $h_{r,k}, h_{q,k}, q_i$ from Problem (17) with $2M$ additional entries. These additional entries correspond to the coefficients of the slack variables u , at most one of which is involved in each constraint.

3.2. Application of DC programming

In order to apply DC programming to solve (19), both (19a) and (19b) have to be written as a difference of two convex functions as described in (9). We call this procedure a “DC

split". Since (19a) is linear, no split has to be performed, we can just define $g_0(x) := c^T x$ and $h_0(x) := 0$. The constraints (19b) on the other hand can be non-convex, so they have to be separated. Note that for every symmetric indefinite matrix P , there exist infinitely many pairs $P^+, P^- \succeq 0$ such that

$$P = P^+ - P^-. \quad (21)$$

As a consequence, problem (19) can be rewritten as

$$\underset{x}{\text{minimize}} \quad c^T x \quad (22a)$$

$$\text{subject to} \quad (x^T P_i^+ x + p_i^T x + \omega_i) - (x^T P_i^- x) \leq 0, \quad (22b)$$

$$i \in \{1, \dots, K\},$$

$$x_j \geq 0, \quad (22c)$$

$$j \in \{2M + 1, \dots, 4M\},$$

which now has the form given in (9). Therefore, the algorithm from Figure 1 can directly be applied.

The existence of infinitely many splits of the P matrices from (19) raises the question of optimal split selection. One approach that both intuitively makes sense and has been effective in experiments is to split the matrices such that the P_i^- have small eigenvalues. This split strategy leads to the curvature of the concave terms $-x^T P_i^- x$ being smaller and therefore the linearized approximation being closer to the original non-convex term. One can also use the freedom in the splits to induce structure in the Hessian matrix P_i^+ in order to simplify the convex problems to be solved. For example, the structure imposed here is for the matrices P_i^+ to be diagonal, making their inverses trivial to compute.

3.3. Analytic eigenvalue computations

Since there are a large number of constraints of the type (19b), calculating splits using numerical eigenvalue decompositions would be computationally prohibitive. Due to the structure of the P_i , eigenvalues can be computed analytically using the method described in this section. Note first that for the indexes i corresponding to voltage or line constraints, the eigenvalues of P_i are trivial to compute due to their simple structure. For the power constraints, we use the following Lemma:

Lemma 1. *The eigenvalues of the matrices from (18) are given by*

$$\text{eig}(\hat{H}_{r,k}) = \left\{ \frac{\text{Re}(Y_{kk}) \pm \sqrt{\text{Re}(Y_{kk})^2 - 4\|Y^{(k)}\|_2^2}}{2}, 0 \right\}, \quad (23a)$$

$$\text{eig}(\hat{H}_{q,k}) = \left\{ \frac{-\text{Im}(Y_{kk}) \pm \sqrt{\text{Im}(Y_{kk})^2 - 4\|Y^{(k)}\|_2^2}}{2}, 0 \right\}. \quad (23b)$$

Proof. The proof is shown for $\hat{H}_{r,k}$ only, since the proof for the $\hat{H}_{q,k}$ is identical. Note first that the $\hat{H}_{r,k}$ have a blocked structure:

$$\hat{H}_{r,k} = \begin{bmatrix} A_k & B_k \\ -B_k & A_k \end{bmatrix} = \begin{bmatrix} A_k & B_k \\ B_k^T & A_k \end{bmatrix}. \quad (24)$$

For matrices of this form, the identity

$$\text{eig}(A_k + \sqrt{-1}B_k) = \text{eig}\left(\begin{bmatrix} A_k & B_k \\ -B_k & A_k \end{bmatrix}\right), \quad (25)$$

holds [13]. Both A_k and B_k are permuted arrowhead matrices. A matrix $A \in \mathbb{C}^{m \times m}$ is called *arrowhead* if it has a structure

$$A = \begin{bmatrix} \alpha & a^T \\ b & D \end{bmatrix}, \quad (26)$$

with $\alpha \in \mathbb{C}$, $a, b \in \mathbb{C}^{m-1}$ and $D = \text{diag}(d) \in \mathbb{C}^{(m-1) \times (m-1)}$ for some $d \in \mathbb{C}^{m-1}$. In case $D = 0$, it can easily be shown [24] that

$$\text{eig}(A) = \left\{ \frac{\alpha \pm \sqrt{\alpha^2 + 4a^T b}}{2}, 0 \right\}. \quad (27)$$

Next, note that A_k only has one non-zero row at the same index as B_k has its only non-zero row, and the same holds for their columns. This means that $A_k + \sqrt{-1}B_k$ is also arrowhead and its eigenvalues are the same as those of $\hat{H}_{r,k}$ due to (25). Substituting $A_k = \text{Re}(Y^{(k)})$, $B_k := \text{Im}(Y^{(k)})$ and applying (27) yields the lemma. \square

Note that the application of (27) is particularly simple for the case here, since $\hat{H}^{r,k}$ is built from $Y^{(k)}$, which in turn only has as many entries as bus k has neighbors. Since power system graphs are generally very sparse, this yields a significant reduction in computational cost over even a Lanczos-based or other iterative approximation of eigenvalues, let alone a standard exact computation.

3.4. Sparse splits

At this point, the eigenvalues of all the matrices P_i can be computed efficiently. However, directly applying the split in (21) would lead to a loss of sparsity. Due to the sparse graph structure of the grid matrix Y , the expressions $x^T P_i x$ only involve a small subset of the variables in x (specifically, the local variables for a bus and the variables of its neighbors). This section introduces an alternative split that both conserves sparsity in the constraints and also makes the P_i^+ diagonal. This structure will then make the solution of the convex subproblems of the algorithm much simpler, as will be outlined in later sections. This is because the P_i^+ are used in the quadratic parts of the convex subproblems, whereas the P_i^- only appear in their linear terms.

Define a sparse, diagonal matrix D_i as follows:

$$(D_i)_{jj} = \begin{cases} 1, & \text{if } j \in J(P_i) \cup J(p_i), \\ 0, & \text{otherwise.} \end{cases} \quad (28)$$

This matrix hence has ones only at the row and column indexes at which either P_i and p_i also have nonzeros. We then define the alternative split

$$P_i := \alpha D_i - (\alpha D_i - P_i), \quad (29)$$

where α is the absolute value of the largest eigenvalue of P_i . This sparse split still guarantees positive definiteness of the split matrices since it only shifts the non-zero eigenvalues.

4. Efficient solution of inner problems

The bottleneck of the DC algorithm is the solution of the convex approximation. In this section, an dual projected gradient method that has an iteration complexity linear in the problem size. With the splits (29) applied, the problem to be solved at each DC iteration has the form

$$\underset{x \in \mathbb{R}^{4M}, t}{\text{minimize}} \quad c^T x + \beta^k t \quad (30a)$$

$$\text{subject to} \quad x^T P_i^+ x + \hat{p}_i(\tilde{x}^k)^T x + \hat{\omega}_i(\tilde{x}^k) \leq t, \quad (30b)$$

$$i \in \{1, \dots, 10M + L\}, \quad t \geq 0, \quad (30c)$$

$$x_j \geq 0, \quad (30d)$$

$$j \in \{2M + 1, \dots, 4M\},$$

where \tilde{x}^k is the current point around which a convex approximation is formed, and

$$\begin{aligned} \hat{p}_i(\tilde{x}^k) &:= (p_i - 2P_i^- \tilde{x}^k), \\ \hat{\omega}_i(\tilde{x}^k) &:= \omega_i + (\tilde{x}^k)^T P_i^- \tilde{x}^k. \end{aligned} \quad (31)$$

General-purpose sparse convex second-order cone programming codes such as ECOS [8], GUROBI [14] or MOSEK [3] can be used to solve these problems. However, the structure of the problem suggests that a specialized solver could lead to increased performance. Firstly, the constraint Hessians P_i are diagonal and sparse, and all nonzero entries have the same values. Additionally, P_i and p_i have the same nonzero patterns for any given i . It was also experimentally observed that the subsequent convex approximations are often similar, which suggests a warm-startable method could be beneficial. This section will present an approach based on accelerated dual gradient descent that was used in this work.

4.1. Projected gradient method

A well-known algorithm for solving optimization problems of the form

$$\underset{x}{\text{minimize}} \quad f(x) \tag{32a}$$

$$\text{subject to} \quad x \in \mathcal{C} \tag{32b}$$

is given by the iteration

$$x^{(k+1)} = \text{proj}_{\mathcal{C}} \left(x^{(k)} - \alpha \nabla f(x^{(k)}) \right) \tag{33}$$

where α is a step size and $\text{proj}_{\mathcal{C}}$ is the Euclidean projection onto the set \mathcal{C} . If \mathcal{C} and $f(x)$ are convex, this algorithm converges to the global minimum of (32a), given that the step size is small enough. The rate of convergence depends highly on $f(x)$, and the method can be accelerated by varying α (see for example [23, 26]). In order for this algorithm to be efficient, the projection should be a simple operation. In the next section, a reformulation of problem (30) is given that achieves the latter.

4.2. Box-constrained inner problem formulation

The intersection of the constraints in (30) is not easy to project onto, hence direct application of (33) is not efficient. Using two reformulations, the problem will be recast as a minimization of a smooth function subject to box constraints. The first step is a lifting into a higher-dimensional variable space: We introduce variables $y_i := x_i^2$ and change the penalty function from an ∞ -norm to a 1-norm (another possible penalty function shown in [20]). The inner problem to be solved then becomes

$$\underset{x,y,t}{\text{minimize}} \quad c^T x + \beta^k \mathbf{1}^T t \tag{34a}$$

$$\text{subject to} \quad Ax + By - b \leq t, \tag{34b}$$

$$\text{diag}(x)x - y = 0, \tag{34c}$$

$$t \geq 0, \tag{34d}$$

$$x_j \geq 0, \tag{34e}$$

$$j \in \{2M + 1, \dots, 4M\},$$

where

$$A := \begin{bmatrix} \hat{p}_1(\tilde{x}^k)^T \\ p_2(\tilde{x}^k)^T \\ \vdots \\ p_K(\tilde{x}^k)^T \end{bmatrix}, \quad B := \begin{bmatrix} \text{diag}(P_1^+)^T \\ \text{diag}(P_2^+)^T \\ \vdots \\ \text{diag}(P_K^+)^T \end{bmatrix}, \quad b := \begin{bmatrix} \hat{\omega}_1(\tilde{x}^k) \\ \omega_2(\tilde{x}^k) \\ \vdots \\ \omega_K(\tilde{x}^k) \end{bmatrix}, \tag{35}$$

where $K := 10M + L$. We now make use of the following lemma to relax the constraints in (34c):

Lemma 2. Consider a version (P) of (34) with the constraints (34c) relaxed to

$$\text{diag}(x)x - y \leq 0. \quad (36)$$

For every minimizer of (P) with one or more of (36) inactive, a minimizer with equal cost function can be found which has all the constraints (36) active.

Proof. The lemma will be shown by construction: Assume a point (x^*, y^*, t^*) is optimal for (P), but a constraint in (36) is not active. Then the y_i corresponding to that constraint can be decreased to make the constraint active without any change to the cost function or constraint satisfaction. The latter is due to all entries of B being non-negative. \square

Lemma 2 implies that we can simply solve the relaxed version of (34) and then recover an optimal solution for the latter. In a second step, the relaxed version of (34) will be dualized to yield a box-constrained problem. With some additional reformulation (see Appendix A.1), the dual of (34) can be written as

$$\underset{\lambda}{\text{minimize}} \quad \frac{1}{4} \lambda^T C (\text{diag}(D^T \lambda)^{-1}) C^T \lambda + d^T \lambda \quad (37a)$$

$$\text{subject to } 0 \leq \lambda \leq 1. \quad (37b)$$

for C, D, d as derived in the appendix. This problem can now readily be solved using the projected gradient method and its accelerated variants: The cost function is a sum of “quadratic over linear” functions, which are convex and differentiable:

$$\frac{\partial}{\partial \lambda} \left(\frac{(a^T \lambda)^2}{b^T \lambda} \right) = 2a \frac{a^T \lambda}{b^T \lambda} - b \frac{(a^T \lambda)^2}{(b^T \lambda)^2}.$$

In order to avoid numerical issues with the inverse of $\text{diag}(D^T \lambda)$, a term εy can be added to (34a) for a small $\varepsilon > 0$. This leads to the inverse in (37a) becoming $\text{diag}(D^T \lambda + 1\varepsilon)^{-1}$, which is well-defined for all $\lambda \geq 0$. Since the Lipschitz constant of (37a) is not easily derived, an adaptive backtracking line search was used to determine the step size α taken in (33). The initial guess for the step size was chosen to be 2 times the step size taken in the previous iteration. This allows the algorithm to adapt its initial guess to both growing as well as shrinking step sizes. At the same time, no convergence guarantees are lost since the line search is still performed at each iteration. This technique led to a significant reduction in the average number of line search iterations, speeding up the overall algorithm substantially.

4.3. Computational complexity

In order to investigate how scalable the presented method is, it is worthwhile to compute the iteration complexity of the inner solver based on the problem parameters. Let d_{\max} be the maximum number of neighbors of any vertex in the power system graph, and recall that the number of buses and lines are denoted by M and L , respectively. The

rows of the matrices C and D ultimately come from the $Y^{(k)}$ and variations thereof. Each of them has at most $2d_{\max}$ entries. Since the number of rows in C and D is $\mathcal{O}(M + L)$, this translates to the number of entries being $\mathcal{O}((M + L)d_{\max})$. All that is required for the cost function and gradient computations is products of C^T and D^T with λ as well as some vector operations. The projection is an elementwise operation and therefore $\mathcal{O}(M + L)$. In summary, an iteration of the inner solver has linear complexity in the size of the grid if d_{\max} is assumed to only grow very weakly with system size, which is true in all test cases available.

5. Numerical results

In this section, we present numerical results on the performance and behavior of the proposed algorithm. In order to make the results comparable to other work in the field, some of the tests will be conducted on the IEEE benchmark test systems available in MATPOWER [10, 35]. For the experiments, a standalone implementation of the proposed method was created, which will be referred to as DQ-OPF. The implementation is a single-threaded, library-free ANSI C code, compiled with GNU GCC. The test computer had a Core i7-4600U dual-core CPU clocked at 2.1 GHz and 8 GB of memory. The operating system used was Debian Linux.

5.1. Algorithm behavior

In the first set of results, the convergence behavior of the algorithm is investigated. For these problems, a local optimum (v^*, s^*) was found with IPOPT [33]. The entries of v^* were then perturbed uniformly and the corresponding perturbed powers were computed using the Kirchhoff equations to yield a perturbed operating point (\tilde{v}, \tilde{s}) . The perturbation size was chosen to make the maximum constraint violation about 100%. This was done in order to simulate the practical situation of the power grid state being only slightly infeasible with respect to the operational constraints, but respecting the Kirchhoff equations. The point (\tilde{v}, \tilde{s}) was used as starting point (s^0, v^0) as defined in Section 2.2, and DQ-OPF started from there.

An example solver run is shown in Figure 3 with a termination criterion of $\|x^k - x^{k-1}\|_2 \leq 10^{-4}$. Within a small number of DC iterations, the maximum constraint violation of the non-convex problem drops below 10^{-4} per unit, which is well below 1% relative accuracy. Note also that the objective value does not improve significantly past iteration 5.

For the problem shown in Figure 3, the inner convex problems were solved to high accuracy (10^4 inner iterations). In other sequential convex programming methods, it is often observed that solving the intermediate problems approximately can often be sufficient for convergence [15]. In order to investigate if this is also the case with the methods presented here, the gradient solver iterations were limited to 100 in the same problem as above, and the other parameters left unchanged. The resulting run for the same problem is shown in Figure 4. While the number of outer iterations required is higher than before for the same accuracy, they are two orders of magnitude cheaper

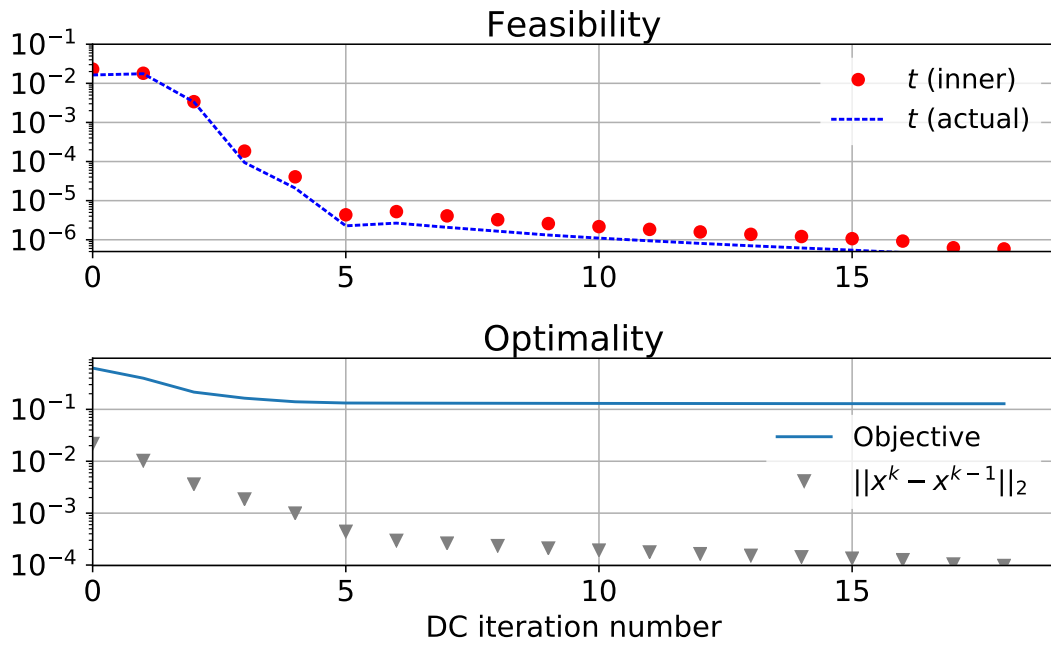


Fig. 3: The DC method applied to the MATPOWER version of the IEEE 30-bus grid, using dual projected gradient as the inner solver. The “ t (inner)” line represents the maximum constraint violation of the convex approximation at that iteration, whereas the “ t (actual)” represents the maximum constraint violation of the original, non-convex problem. The lower subplot shows the true objective as well as the difference between subsequent iterates.

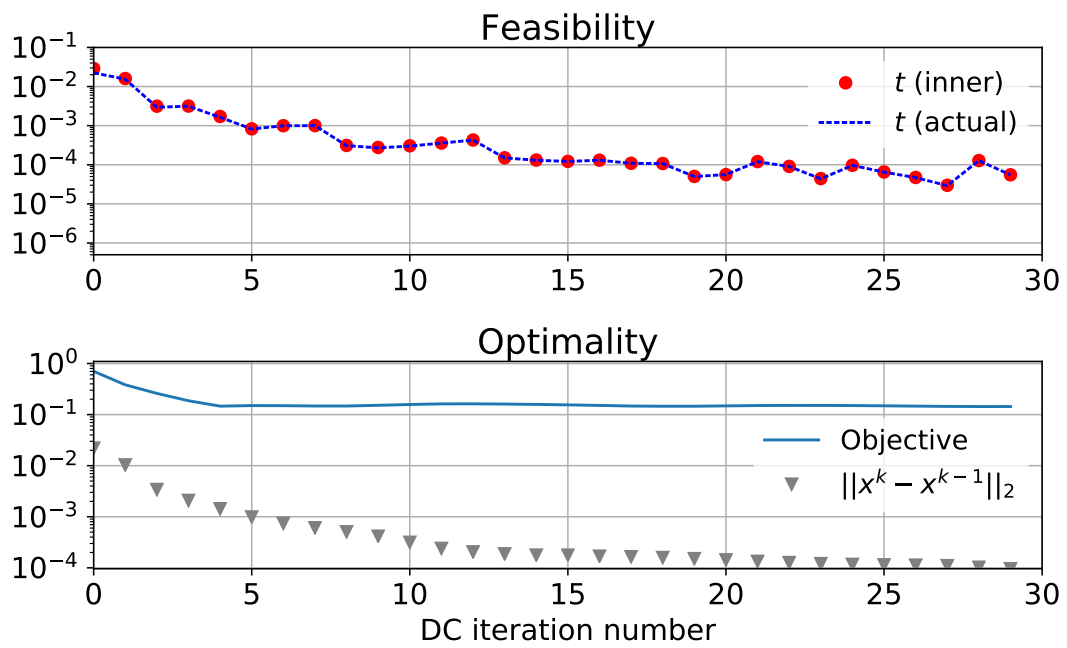


Fig. 4: Solution of the same problem as in Figure 3, but with the accuracy for the inner problem severely limited. The optimal value of the inner problems no longer decreases monotonically, due to the inaccurate inner solutions.

Table 1: Average time and objective for 1% relative accuracy

	IPOPT & PARDISO		DQ-OPF	
	Time	Objective	Time	Objective
6-bus	55 ms	0.9	2.2 ms	0.9
9-bus	65 ms	1.9	2.3 ms	1.5
14-bus	68 ms	1.3	3.5 ms	1.0
30-bus	77 ms	1.5	10 ms	1.3
39-bus	92 ms	12	23 ms	11
57-bus	97 ms	2.9	25 ms	1.6
118-bus	213 ms	17	76 ms	3.7
2383-bus	3.5 s	24	4.4 s	10.4
2737-bus	3.3 s	12	2.4 s	7.6
3210-bus	2.8 s	14	4.0 s	9.2
9241-bus	15 s	26	16 s	6.8

computationally. Note that the objectives in Figure 3 and Figure 4 converge to slightly different values. This is due to the two solver runs converging to different local optima.

5.2. Performance

In order to compare the implemented method to the state of the art, MATPOWER test cases were used in conjunction with the 1-norm cost function, as described in (8). Instead of solving the inner problems accurately as shown in Figure 3, the inner solver was limited to 100–1000 iterations depending on grid size, yielding the aforementioned calculation time improvements. The DC solver parameters were tuned for one instance of the problem and then reused across all runs. The solver was started at (s^0, v^0) . As a reference, we used MATPOWER’s IPOPT interface along with the parallel PARDISO [18, 28, 29] solver for linear systems. Table 1 presents the results averaged over 100 runs with random initial points created as in the previous experiment. In these experiments, IPOPT was warm-started at the same point as DQ-OPF using MATPOWER’s warm-start functionality. DQ-OPF is faster in many cases, with the speedups for the smaller grids being substantial. For the larger grids, the run times are comparable to the reference. Since no significant effort was put into optimizing the solver for larger grids, further speedups can be expected in the proposed method through parallelization and more efficient code. For the largest grid, MATPOWER ran into memory issues on the computer used. DQ-OPF requires a memory amount linear in the problem size and hence had no such issues. Note also that IPOPT was run with multi-threading enabled (2 threads) and the times shown are wall clock, not CPU time.

Another observation is that the average objective values were consistently smaller

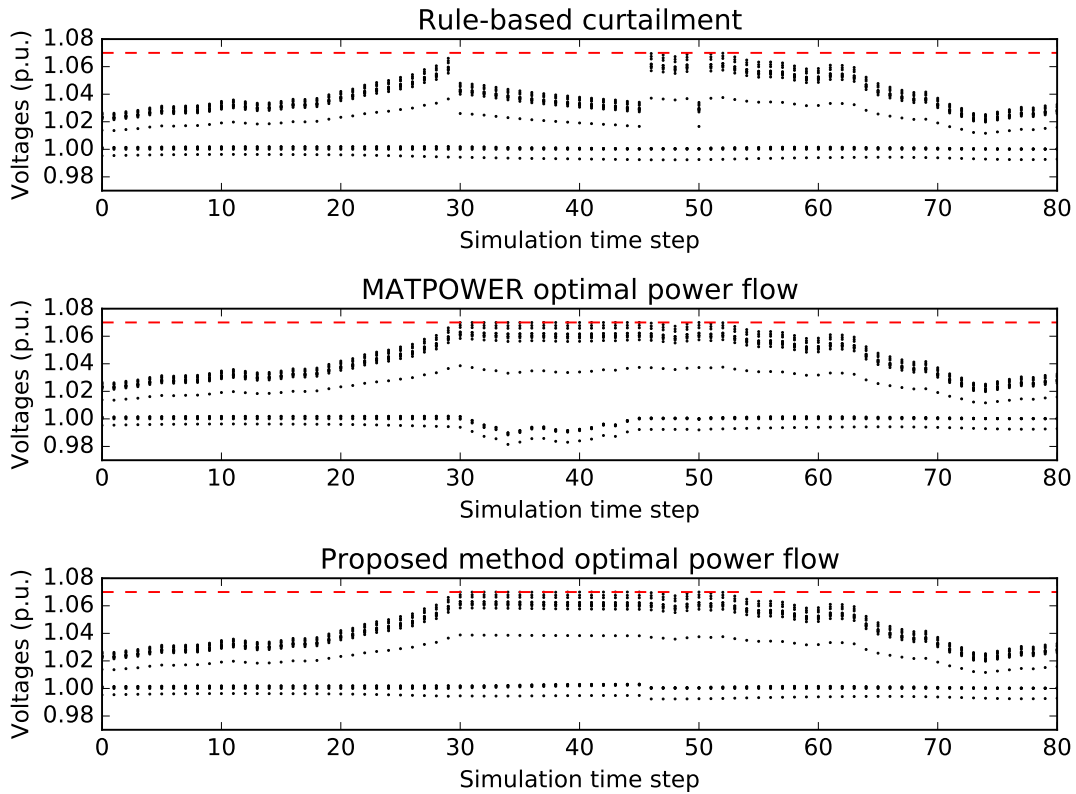


Fig. 5: Voltage traces for all buses in the MV grid over the course of the simulation. Admissible limits were $[0.9, 1.07]$ per unit. The OPF problem had to be solved at time instances 30 through 25 and 50.

with the method used. This means the proposed method found local optima with better objective values. A likely reason for this is the objective function, which represents distance from the starting point (s^0, v^0) . The presented method tends to find local optima close to the point at which it was started, whereas IPOPT (and interior-point methods in general) seem to benefit less from warm-start information [16]. This difference in objective values was made both when IPOPT was warm-started as well as when the default settings (no warm-start) were used.

5.3. Case study: Simulation experiment

In order to demonstrate the effectiveness of warm-starting the presented method, a power system time simulation experiment is presented in this section. The experiment was run with the test grid shown in Figure 7. Three different approaches to dealing with voltage violations were tested:

- (i) *Rule-based curtailment*: In this control scheme, no optimization is run, instead the

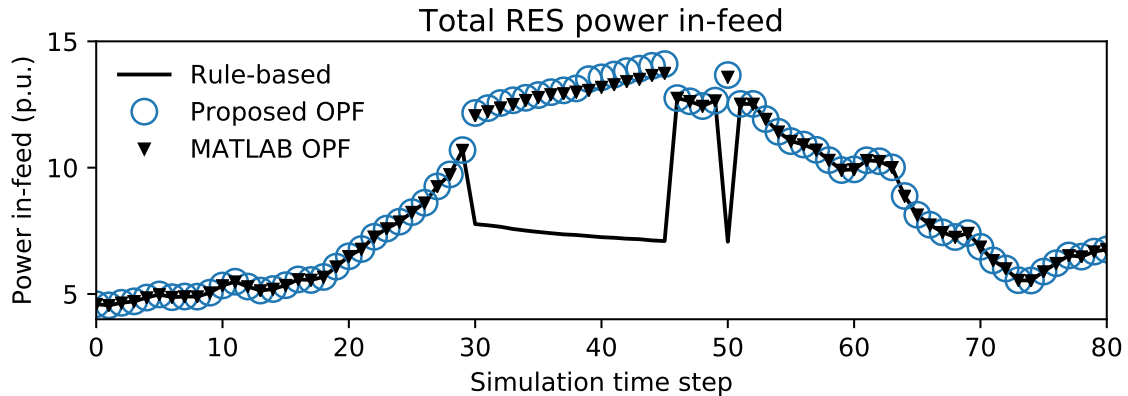


Fig. 6: Total RES power in-feed for the MV grid over the simulation horizon. The MATPOWER and proposed OPF solutions are close, with the proposed solution discarding slightly less renewable energy.

renewable in-feeds of the grid are simply curtailed down to a fixed fraction of their rated in-feed. This case reflects current industry practice.

- (ii) *MATPOWER OPF-based curtailment*: In this scheme, problem (8) is solved to local optimality with MATPOWER at its default settings. The 1-norm cost was implemented using MATPOWER’s piecewise affine cost function functionality.
- (iii) *Proposed method OPF-based curtailment*: Problem (8) is solved to local optimality, but with the method presented in this paper. The solver is warm-started with the solution from the previous solve when available. The inner problems were solved with the presented dual gradient method, which was limited to 200 inner iterations.

As a simulation environment, Adaptricity DPG.sim [17] was used. At each simulation time step, the operational limits (2), (5) and (6) were checked. If any of them were violated, one of the approaches above was invoked. The resulting power in-feed and voltage profiles for the different approaches are shown in Figures 5 and 6, respectively. As can be seen in the uppermost subplots of the two figures, the profiles obtained by using the rule-based curtailment controller have strong fluctuations due to the controller intervening non-smoothly when violations are detected. Both the voltage and power profiles are much smoother if the optimization-based intervention solving (8) is performed. Even though only local optima are found both in MATPOWER and the presented method, these smoother profiles were observed in all simulations. Additionally, even though the different numerical approaches often yield different local minima, the difference in cost function values is minor. The distribution of solve times for the simulation is presented in Figure 8. As can be seen, the average solve time of the proposed method is only about 14% of the state of the art. This directly results in a speedup of up to factor 7 in the simulations.

Finally, due to the less severe interventions, much less curtailment is required, resulting in a significant increase of renewable energy integrated. The typical increase in RES in-

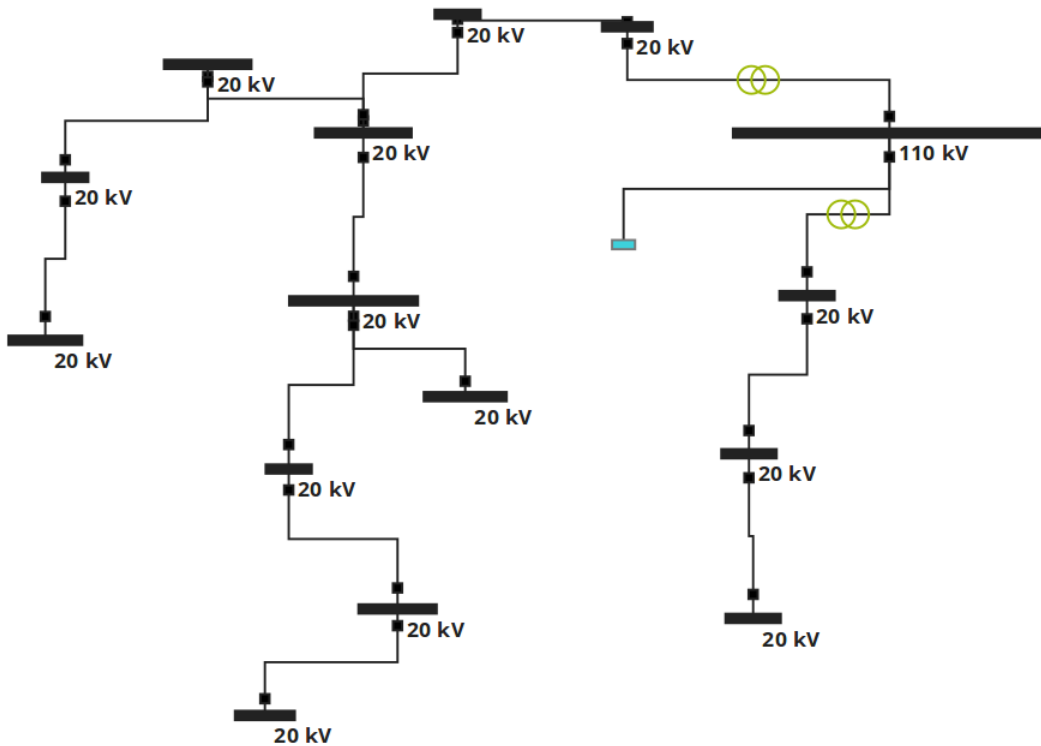


Fig. 7: Rural MV grid used for the simulation experiment. Line admittances were chosen to be in range typically used in rural distribution grids. Note that while the grid here is radial, this is not a required assumption for the proposed method. The cyan bus in the middle is the slack bus, modeled here as a bus with no power limits.

feed is in the 20–40% in yearly simulations, but the specific value depends strongly on the grid topology and available amount of renewable in-feed capacity.

6. Conclusion

This paper presented an alternative approach to dealing with over-voltage problems in distribution grids with an OPF-based approach that leads to minimum intervention by the DSO. Along with a formulation of the optimization problem, a novel method to solve it to local optimality was presented that can be warm-started and significantly outperforms current state-of-the-art interior-point methods. The presented method can easily be extended to other optimization problems involving AC power flow constraints.

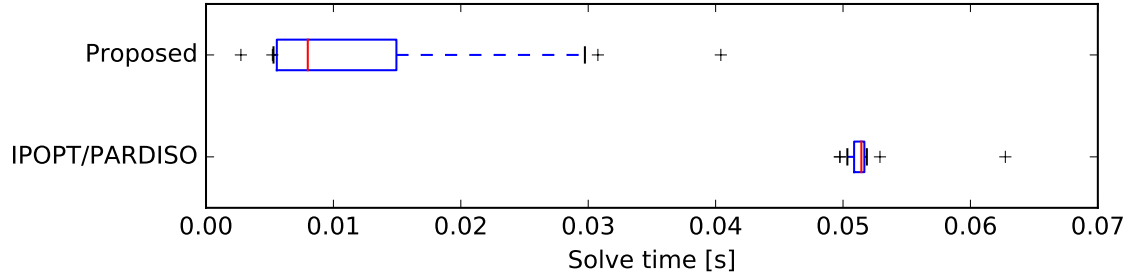


Fig. 8: Box-plot of the distribution of solve times for the optimization problems solved in the simulation experiment. The boxes contain 50% of the cases, the interval marked by the dashed lines contains 90% of the cases. The plus signs mark outliers.

Acknowledgments

This work was supported by the Swiss Commission for Technology and Innovation (CTI), (Grant 16946.1 PFIW-IW). We also thank the team at Adaptricity (Stephan Koch, Andreas Ulbig and Francesco Ferrucci) for providing the simulation environment and valuable discussions in the area of power systems.

A. Appendix

A.1. Derivation of the dual problem

In this section, a detailed derivation of the step from (34) to (37) is given. First, notice that the only non-zeros entries of c in (34) are those corresponding to the slack variables u introduced in (19). Moreover, the constraints corresponding to the cost function reformulation do not need penalties, since they are satisfied by construction. Recalling $x = [z^T \ u^T]^T$, we can rewrite (34) as

$$\underset{x,y,u,t}{\text{minimize}} \quad 1^T u + \beta^k 1^T t \quad (38a)$$

$$\text{subject to} \quad A_1 z + B_1 y - b_1 \leq t, \quad (38b)$$

$$A_2 z + B_2 y - b_2 \leq u, \quad (38c)$$

$$\text{diag}(z)z - y \leq 0, \quad (38d)$$

$$t \geq 0, \quad (38e)$$

$$u \geq 0. \quad (38f)$$

In (38), constraints (38b) contain all the actual constraints (originally (17b)), whereas (38c) contains all constraints resulting from the cost function reformulation. In the 1-norm cost formulation, a trick has been applied: Normally, a cost of $|w|$ for some variable w

would be replaced by one slack variable s and then a problem

$$\begin{aligned} & \underset{w,s}{\text{minimize}} && s + (\text{other costs}) \\ & \text{subject to} && w \leq s, \quad -w \leq s, \\ & && (\text{other constraints}), \end{aligned}$$

solved. An equivalent formulation to this is to introduce two slack variables s_1, s_2 and solve

$$\begin{aligned} & \underset{w,s}{\text{minimize}} && s_1 + s_2 + (\text{other costs}) \\ & \text{subject to} && w \leq s_1, \quad -w \leq s_2, \\ & && s_1 \geq 0, \quad s_2 \geq 0, \\ & && (\text{other constraints}). \end{aligned}$$

The equivalence is easily shown: One of $-w, w$ is always negative, leading to one of s_1, s_2 becoming 0, and the cost being equivalent to the more standard formulation. Because this alternative formulation was used, one can treat the t and u in (38) the same and rewrite the latter once more as

$$\underset{x,y,t}{\text{minimize}} \quad 1^T t \tag{39a}$$

$$\text{subject to} \quad Cz + Dy - d \leq t, \tag{39b}$$

$$\text{diag}(z)z - y \leq 0, \tag{39c}$$

$$t \geq 0, \tag{39d}$$

$$\tag{39e}$$

where t now has a larger dimension than the t in (38) and

$$C := \begin{bmatrix} \beta^k A_1 \\ A_2 \end{bmatrix}, \quad D := \begin{bmatrix} \beta^k B_1 \\ B_2 \end{bmatrix}, \quad d := \begin{bmatrix} \beta^k b_1 \\ b_2 \end{bmatrix}.$$

At this point, let λ, μ and γ be the dual multipliers for the constraints (39b), (39c) and (39d), respectively. The Lagrangian of (39) then becomes

$$\begin{aligned} L(z, y, t, \lambda, \mu, \gamma) = & 1^T t + \lambda^T (Cz + Dy - d - t) \\ & + \mu^T (\text{diag}(z)z - y) + \gamma(-t). \end{aligned} \tag{40}$$

Setting the partial derivatives to 0 yields

$$1 - \lambda - \gamma = 0, \tag{41a}$$

$$C^T \lambda + 2 \text{diag}(\mu)z = 0, \tag{41b}$$

$$D^T \lambda - \mu = 0. \tag{41c}$$

Equation (41b) implies that

$$z^*(\lambda, \mu) = -\frac{1}{2} \text{diag}(\mu)^{-1} C^T \lambda.$$

The dual problem hence becomes

$$\underset{x,y,t}{\text{maximize}} \quad -\frac{1}{4}\lambda^T C \text{diag}(\mu)^{-1} C^T \lambda - d^T \lambda \quad (42a)$$

$$\text{subject to } \lambda, \gamma, \mu \geq 0, \quad (42b)$$

$$1 - \lambda - \gamma = 0, \quad (42c)$$

$$D^T \lambda - \mu = 0. \quad (42d)$$

Upon closer inspection of (42), it can be seen that γ and μ can be eliminated to yield

$$\underset{x,y,t}{\text{maximize}} \quad -\frac{1}{4}\lambda^T C \text{diag}(D^T \lambda)^{-1} C^T \lambda - d^T \lambda \quad (43a)$$

$$\text{subject to } 0 \leq \lambda \leq 1, \quad (43b)$$

$$D^T \lambda \geq 0. \quad (43c)$$

Finally, since all entries of D are non-negative, constraints (43b) imply (43c), and the latter can therefore be removed, resulting in the formulation (37) presented in the main text.

References

- [1] O. Alsac, J. Bright, M. Prais, and B. Stott. Further developments in LP-based optimal power flow. *IEEE Transactions on Power Systems*, 5(3):697–711, Aug 1990.
- [2] LeThiHoai An and PhamDinh Tao. The DC (Difference of Convex Functions) Programming and DCA Revisited with DC Models of Real World Nonconvex Optimization Problems. *Annals of Operations Research*, 133(1-4):23–46, 2005.
- [3] ApS. *The MOSEK C optimizer API manual Version 7.0*, 2015.
- [4] H.M. Ayres, W. Freitas, M.C. De Almeida, and L.C.P. Da Silva. Method for determining the maximum allowable penetration level of distributed generation without steady-state voltage violations. *IET Generation, Transmission & Distribution*, 4:495–508(13), April 2010.
- [5] Mokhtar S Bazaraa, Hanif D Sherali, and Chitharanjan M Shetty. *Nonlinear Programming: Theory and Algorithms*. John Wiley & Sons, 2013.
- [6] BMWI. Gesetz für den Ausbau erneuerbarer Energien (EEG). [Online]. Available: <http://www.bmwi.de>, 2014.
- [7] Show-Kang Chang, Farrokh Albuyeh, Michel L Gilles, George E Marks, and Ken Kato. Optimal real-time voltage control. *IEEE Transactions on Power Systems*, 5(3):750–758, 1990.

- [8] A. Domahidi, E. Chu, and S. Boyd. ECOS: An SOCP solver for embedded systems. In *European Control Conference (ECC)*, pages 3071–3076, Zurich, Switzerland, 2013.
- [9] ENTSO-E. Operation handbook. [Online]. Available: <http://www.entsoe.eu>, 2004.
- [10] Stéphane Fliscounakis, Patrick Panciatici, Florin Capitanescu, and Louis Wehenkel. Contingency ranking with respect to overloads in very large power systems taking into account uncertainty, preventive, and corrective actions. *Power Systems, IEEE Transactions on*, 28(4):4909–4917, 2013.
- [11] Stephen Frank, Ingrida Steponavice, and Steffen Rebennack. Optimal power flow: A bibliographic survey I. *Energy Systems*, 3(3):221–258, 2012.
- [12] Stephen Frank, Ingrida Steponavice, and Steffen Rebennack. Optimal power flow: A bibliographic survey II. *Energy Systems*, 3(3):259–289, 2012.
- [13] G.H. Golub and C.F. Van Loan. *Matrix Computations*. Johns Hopkins University Press, 2012.
- [14] Inc. Gurobi Optimization. *Gurobi Optimizer Reference Manual*, 2014.
- [15] Matthias Heinkenschloss and Luis N Vicente. Analysis of inexact trust-region SQP algorithms. *SIAM Journal on Optimization*, 12(2):283–302, 2002.
- [16] Elizabeth John and E.Alper Yildirim. Implementation of warm-start strategies in interior point methods for linear programming in fixed dimension. *Computational Optimization and Applications*, 41(2):151–183, 2008.
- [17] Stephan Koch, Francesco Ferrucci, Andreas Ulbig, and Michael Koller. Time-series simulations and assessment of smart grid planning options of distribution grids. In *Proceedings of the CIRED Workshop*, Rome, Italy, 2014.
- [18] A. Kuzmin, M. Luisier, and O. Schenk. Fast methods for computing selected elements of the greens function in massively parallel nanoelectronic device simulations. In F. Wolf, B. Mohr, and D. Mey, editors, *Euro-Par 2013 Parallel Processing*, volume 8097 of *Lecture Notes in Computer Science*, pages 533–544. Springer Berlin Heidelberg, 2013.
- [19] J. Lavaei and S.H. Low. Zero duality gap in optimal power flow problem. *IEEE Transactions on Power Systems*, 27(1):92–107, Feb 2012.
- [20] HoaiAn Le Thi, VanNgai Huynh, and TaoPham Dinh. DC Programming and DCA for General DC Programs. In *Advanced Computational Methods for Knowledge Engineering*, volume 282 of *Advances in Intelligent Systems and Computing*, pages 15–35. Springer International Publishing, 2014.
- [21] Steven H Low. Convex Relaxation of Optimal Power Flow, Part I: Formulations and Equivalence. *arXiv preprint arXiv:1405.0766*, 2014.

- [22] D.K. Molzahn, J.T. Holzer, B.C. Lesieutre, and C.L. DeMarco. Implementation of a large-scale optimal power flow solver based on semidefinite programming. *IEEE Transactions on Power Systems*, 28(4):3987–3998, Nov 2013.
- [23] Yurii Nesterov. A method of solving a convex programming problem with convergence rate $o(1/k^2)$. In *Soviet Mathematics Doklady*, volume 27, pages 372–376, 1983.
- [24] D.P O’Leary and G.W Stewart. Computing the eigenvalues and eigenvectors of symmetric arrowhead matrices. *Journal of Computational Physics*, 90(2):497 – 505, 1990.
- [25] Ren21. Renewables 2015: Global status report. [Online]. Available: <http://www.ren21.net/>, 2015.
- [26] Stefan Richter. *Computational Complexity Certification of Gradient Methods for Real-Time Model Predictive Control*. PhD thesis, ETH Zurich, 2012.
- [27] StephenM. Robinson. A quadratically-convergent algorithm for general nonlinear programming problems. *Mathematical Programming*, 3(1):145–156, 1972.
- [28] Olaf Schenk, Matthias Bollhöfer, and Rudolf A. Römer. On Large-Scale Diagonalization Techniques for the Anderson Model of Localization. *SIAM Rev.*, 50(1):91–112, February 2008.
- [29] Olaf Schenk, Andreas Wächter, and Michael Hagemann. Matching-based preprocessing algorithms to the solution of saddle-point problems in large-scale nonconvex interior-point optimization. *Computational Optimization and Applications*, 36(2-3):321–341, 2007.
- [30] G.L. Torres and V.H. Quintana. On a nonlinear multiple-centrality-corrections interior-point method for optimal power flow. *IEEE Transactions on Power Systems*, 16(2):222–228, May 2001.
- [31] Andreas Ulbig and Göran Andersson. On operational flexibility in power systems. In *Power and Energy Society General Meeting*, pages 1–8, San Diego, CA, USA, 2012. IEEE.
- [32] Evangelos Vrettos, Frauke Oldewurtel, Matteo Vasirani, and Goran Andersson. Centralized and decentralized balance group optimization in electricity markets with demand response. In *PowerTech*, pages 1–6, Grenoble, France, 2013. IEEE.
- [33] Andreas Wächter and Lorenz T Biegler. On the implementation of an interior-point filter line-search algorithm for large-scale nonlinear programming. *Mathematical programming*, 106(1):25–57, 2006.
- [34] J. Warrington, C. Hohl, P.J. Goulart, and M. Morari. Optimal unit commitment accounting for robust affine reserve policies. In *American Control Conference (ACC), 2014*, pages 5049–5055, Portland, OR, USA, June 2014.

- [35] R.D. Zimmerman, C.E. Murillo-Sánchez, and R.J. Thomas. MATPOWER: Steady-State Operations, Planning, and Analysis Tools for Power Systems Research and Education. *IEEE Transactions on Power Systems*, 26(1):12–19, Feb 2011.